SLAC-PUB-11183
*BABAR*-PROC-05/10
June 2005

# Unitarity Triangle Angle Measurements at *BABAR*

Thomas E. Latham
(representing the *BABAR* Collaboration)
*Department of Physics, University of Warwick,*
*Coventry, CV4 7AL, United Kingdom*

## Abstract

We present recent results of measurements of the Unitarity Triangle angles $\alpha$, $\beta$ and $\gamma$ made with the *BABAR* detector at the PEP-II asymmetric $B$ Factory.

*Contributed to 19th Rencontres De Physique De La Vallee D'Aoste,*
*27 Feb - 5 Mar 2005, La Thuile, Aosta Valley, Italy*

*Stanford Linear Accelerator Center, Stanford University, Stanford, CA 94309*

Work supported in part by Department of Energy contract DE-AC02-76SF00515.

# 1 Introduction

The measurements of the angles $\alpha$, $\beta$ and $\gamma$ of the Unitarity Triangle at the *BABAR* and Belle experiments are providing precision tests of the description of *CP* violation in the Standard Model (SM). This description is provided by the Cabibbo-Kobayashi-Maskawa (CKM) quark-mixing matrix[1], which relates the weak and flavour eigenstates of the quarks in the weak Lagrangian

$$\mathcal{L}_{\rm CC} = -\frac{g}{\sqrt{2}}\left(\overline{u}_L, \overline{c}_L, \overline{t}_L\right)\gamma^\mu V_{\rm CKM}\begin{pmatrix} d_L \\ s_L \\ b_L \end{pmatrix} W_\mu^\dagger + \text{h.c.} \tag{1}$$

where

$$\begin{aligned} V_{\rm CKM} &\equiv \begin{pmatrix} V_{ud} & V_{us} & V_{ub} \\ V_{cd} & V_{cs} & V_{cb} \\ V_{td} & V_{ts} & V_{tb} \end{pmatrix} \\ &\approx \begin{pmatrix} 1-\frac{\lambda^2}{2} & \lambda & A\lambda^3(\rho - i\eta) \\ -\lambda & 1-\frac{\lambda^2}{2} & A\lambda^2 \\ A\lambda^3(1-\rho-i\eta) & -A\lambda^2 & 1 \end{pmatrix} + \mathcal{O}(\lambda^4) \end{aligned} \tag{2}$$

is the $3 \times 3$ CKM matrix shown here in the Wolfenstein parameterisation[2]. The imaginary coefficient $\eta$ is the source of *CP* violation.

The CKM matrix is a unitary matrix and using this condition one can write down several relationships of the following form

$$\sum_i V_{ij}V_{ik}^* = 0 \quad (j \neq k). \tag{3}$$

There are six such equations, each of which represents a triangle in the complex plane. One of these has sides of similar magnitude and also contains some of the least well constrained CKM matrix elements:

$$V_{ud}V_{ub}^* + V_{cd}V_{cb}^* + V_{td}V_{tb}^* = 0. \tag{4}$$

The triangle, rescaled by $\frac{1}{V_{cd}V_{cb}^*}$, is illustrated in fig. 1. The internal angles of the triangle are given by

$$\alpha \equiv \arg\left[-\frac{V_{td}V_{tb}^*}{V_{ud}V_{ub}^*}\right], \quad \beta \equiv \arg\left[-\frac{V_{cd}V_{cb}^*}{V_{td}V_{tb}^*}\right], \quad \gamma \equiv \arg\left[-\frac{V_{ud}V_{ub}^*}{V_{cd}V_{cb}^*}\right]. \tag{5}$$

This paper will review recent measurements of these CKM angles from the *BABAR* collaboration. The *BABAR* detector and the PEP-II accelerator are described in detail elsewhere[3, 4].

# 2 Measurements relating to $\beta$

The primary goal of the *BABAR* experiment was to measure $\sin 2\beta$ in the so called "golden modes" that proceed via the decay $b \to c\overline{c}s$, such as $B^0 \to J/\psi\, K_S^0$. These channels are considered golden since they are not too challenging experimentally and are theoretically clean due to the presence of only one weak phase. The latest *BABAR* measurement using a data sample of 227 million $B\overline{B}$ pairs is: $\sin 2\beta = 0.722 \pm 0.040 \pm 0.023$[5]. Measuring $\sin 2\beta$ results in a four-fold ambiguity on $\beta$ itself but one of the four solutions is in excellent agreement with the predictions of the Standard Model based on experimental knowledge of other parameters, as can be seen from fig. 2.

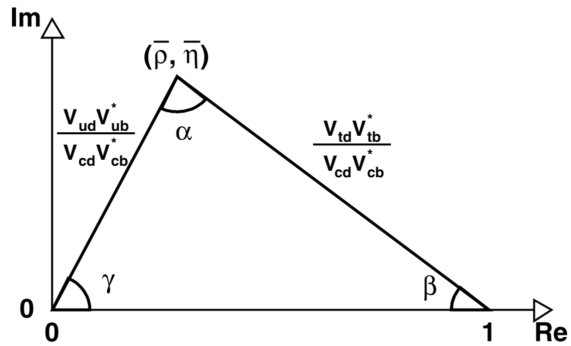


Figure 1: The Unitarity Triangle.

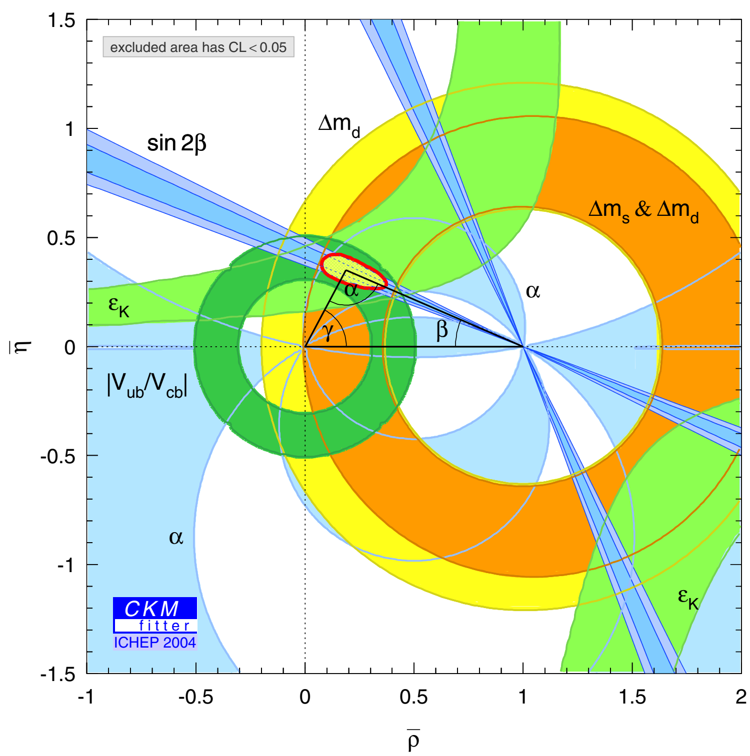


Figure 2: The $\bar{\rho} - \bar{\eta}$ plane showing the various constraints on the Unitarity Triangle.

## 2.1 Measurement of the sign of $\cos 2\beta$

In order to properly test the Standard Model it is important to reduce the ambiguity on the measurement of $\beta$. The existing four-fold ambiguity can be reduced to two-fold by determining the sign of $\cos 2\beta$ [6].

The decay $B \to J/\psi\, K^*$ has a dependence on $\cos 2\beta$ due to the interference of the one $CP$-odd and two $CP$-even components. This dependence appears in the time-dependent angular distributions in the observables:

$$\cos(\delta_{\parallel} - \delta_{\perp}) \cdot \cos 2\beta, \quad \cos(\delta_{\perp} - \delta_0) \cdot \cos 2\beta \tag{6}$$

where $\delta_i$ are the strong phases of the decay amplitudes:

$$A_i = |A_i| e^{i\delta_i}. \tag{7}$$

Using samples of both neutral and charged decays it is possible to measure these strong phases up to a two-fold ambiguity:

$$(\delta_{\parallel} - \delta_0, \delta_{\perp} - \delta_0) \Leftrightarrow (-(\delta_{\parallel} - \delta_0), \pi - (\delta_{\perp} - \delta_0)). \tag{8}$$

Under this transformation $\cos(\delta_{\parallel} - \delta_{\perp})$ and $\cos(\delta_{\perp} - \delta_0)$ change sign and so the two sets of parameters:

$$(\delta_{\parallel} - \delta_0, \delta_{\perp} - \delta_0, \cos 2\beta) \Leftrightarrow (-(\delta_{\parallel} - \delta_0), \pi - (\delta_{\perp} - \delta_0, -\cos 2\beta)) \tag{9}$$

are equivalent, meaning that the sign of $\cos 2\beta$ is still ambiguous.

However, it is known from previous experiments that the $K^*(892)$ is not the only contribution in this region of $K\pi$ mass and that a broad S-wave is also present[7]. This additional contribution also has an associated strong phase, $\delta_S$, and so a new relative phase enters the problem: $\gamma = (\delta_S - \delta_0)$. The ambiguity of eq. (8) now becomes:

$$(\delta_{\parallel} - \delta_0, \delta_{\perp} - \delta_0, \gamma) \Leftrightarrow (-(\delta_{\parallel} - \delta_0), \pi - (\delta_{\perp} - \delta_0), -\gamma). \tag{10}$$

The ambiguity on $\gamma$ can be broken however using Wigner's causality principle[8], which states that the phase of a resonance rotates anticlockwise with increasing mass. Since the phase of the S-wave is moving very slowly in the region of the $K^*(892)$ while the phase of the P-wave is moving very rapidly the relative phase $\gamma$ must rotate clockwise. fig. 3 shows the behaviour of $\gamma$ as a function of $K\pi$ mass for both solutions along with the data from the LASS experiment[7], which shows remarkable agreement with the one solution that also obeys Wigner's principle.

With the strong phase ambiguity broken a time-dependent fit can be performed to the $B^0 \to J/\psi\, K^{*0}(K^0_S \pi^0)$ data sample in order to extract $\cos 2\beta$ and $\sin 2\beta$. With $\sin 2\beta$ floating in the fit the results obtained are:

$$\begin{aligned} \cos 2\beta &= +3.32^{+0.76}_{-0.96} \pm 0.27 \\ \sin 2\beta &= -0.10 \pm 0.57 \pm 0.14. \end{aligned} \tag{11}$$

If $\sin 2\beta$ is fixed to the world average value of 0.731 we obtain:

$$\cos 2\beta = +2.72^{+0.50}_{-0.79} \pm 0.27. \tag{12}$$

If $\cos 2\beta$ and $\sin 2\beta$ are considered to be measuring the same angle $\beta$ then $\cos 2\beta$ should be $\pm 0.68$. A toy Monte Carlo technique is used to determine which of these solutions is more likely. It is found that the positive solution is preferred at the 89% confidence level. The projection of the time dependent fit is shown in fig. 4. This analysis used a sample of 88 million $B\overline{B}$ pairs.

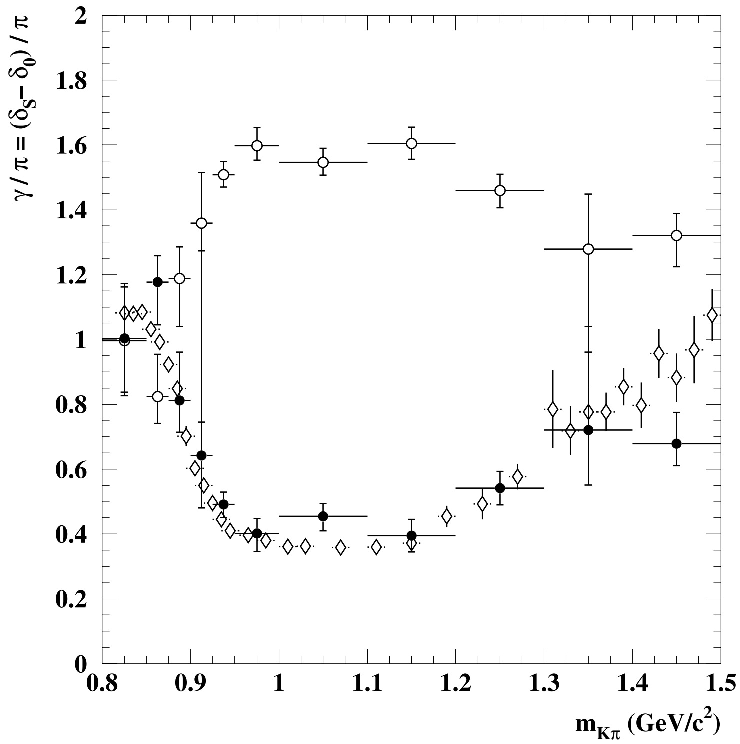


Figure 3: The relative phase $\gamma$ as a function of $K\pi$ mass. The open circles are "Solution 1", the filled circles are "Solution 2" and the open diamonds are the LASS data. A global offset of $\pi$ has been added to the LASS data.

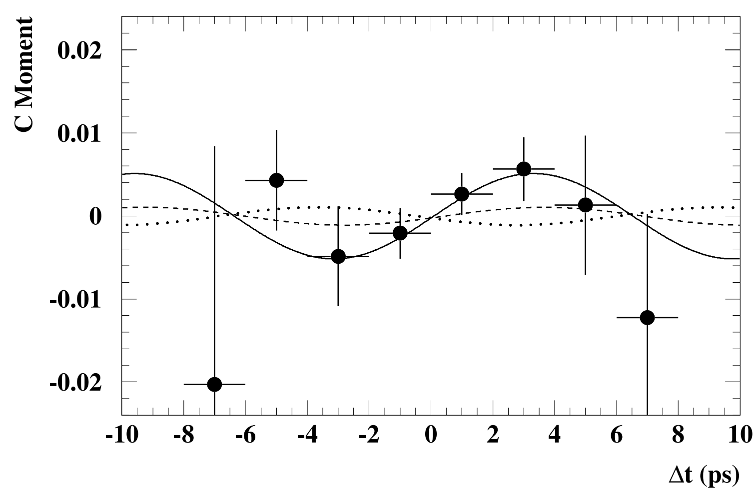


Figure 4: Moment of the function weighting the cos2$\beta$ contribution to the amplitude. The solid line is the result of the fit with both cos2$\beta$ and sin2$\beta$ floating. The dashed line corresponds to the preferred value cos2$\beta = +0.68$ and the dotted to cos2$\beta = -0.68$.

## 2.2 $\sin 2\beta$ from $b \to s\bar{s}s$ Penguin Modes

The time dependent $CP$ asymmetry for a given $B^0/\overline{B}^0$ decay is given by:

$$
\begin{aligned}
A_{f_{CP}}(\Delta t) &= \frac{\Gamma(\overline{B}^0(\Delta t) \to f_{CP}) - \Gamma(B^0(\Delta t) \to f_{CP})}{\Gamma(\overline{B}^0(\Delta t) \to f_{CP}) + \Gamma(B^0(\Delta t) \to f_{CP})} \\
&= \eta_{f_{CP}} S_{f_{CP}} \sin(\Delta m_d \Delta t) - \eta_{f_{CP}} C_{f_{CP}} \cos(\Delta m_d \Delta t)
\end{aligned} \tag{13}
$$

where $\eta_{f_{CP}}$ is the $CP$ eigenvalue of the final state $f_{CP}$, $\Delta m_d$ is the mass difference between the two neutral $B$ mass eigenstates and $\Delta t$ is the time difference between the decays of the two $B$ mesons. Measurements of the $S$ coefficient of this $CP$ asymmetry in decay channels dominated by $b \to s\bar{s}s$ "penguin diagrams" are expected to be equal to $\eta_{f_{CP}} \sin 2\beta$ where $\sin 2\beta$ is that measured in the $b \to c\bar{c}s$ decays. If the measured values are found to deviate then this could be an indication of new particles entering in the loop and contributing to the amplitude. However, care must be taken in the interpretation as small deviations are expected in some modes due to the presence of SM suppressed amplitudes with different weak and strong phases.

### 2.2.1 $B^0 \to \phi K^0_S$ *and* $B^0 \to \phi K^0_L$

This channel is the most theoretically clean of all the penguin modes in that it is expected to have no contribution from tree diagrams. This means that to very good approximation $C_{f_{CP}}$ should be zero and $S_{f_{CP}}$ should be $+\sin 2\beta$ for $\phi K^0_S$ and $-\sin 2\beta$ for $\phi K^0_L$. From a data sample of 227 million $B\overline{B}$ pairs *BABAR* reconstructs $114 \pm 12$ $\phi K^0_S$ events and $98 \pm 18$ $\phi K^0_L$ events. Combining these samples in a time-dependent fit yields the following results[9]:

$$
\begin{aligned}
S_{\phi K^0} &= 0.50 \pm 0.25\,^{+0.07}_{-0.04} \\
C_{\phi K^0} &= 0.00 \pm 0.23 \pm 0.05
\end{aligned} \tag{14}
$$

These results are in good agreement with the SM since $C$ is zero and $S$ is consistent with $\sin 2\beta$ within $1\sigma$.

### 2.2.2 $B^0 \to K^+K^-K^0_S$ *excluding* $\phi K^0_S$

The $B^0 \to K^+K^-K^0_S$ Dalitz plot contains many more events than those simply due to $\phi K^0_S$ and so can reduce the statistical uncertainty on the measurement of $\sin 2\beta$ in these modes. However, there are possible contributions from other amplitudes making it theoretically less clean. Additionally, the $CP$ content of the final state is not known and must be determined. This is achieved using a moments analysis that takes advantage of the statistical technique known as ${}_s\mathcal{P}lot$ [10]. The S- and P-wave intensities are shown in fig. 5 along with the $CP$-even fraction, all as a function of $K^+K^-$ mass. The average number obtained for the $CP$-even fraction was $0.89 \pm 0.08 \pm 0.06$ from the data sample of 227 million $B\overline{B}$ pairs. The time-dependent $CP$ fit then yielded the following results[9]:

$$
\begin{aligned}
S_{K^+K^-K^0_S} &= -0.42 \pm 0.17 \pm 0.03 \\
C_{K^+K^-K^0_S} &= +0.10 \pm 0.14 \pm 0.04 \\
\sin 2\beta_{\text{eff}} &= +0.55 \pm 0.22 \pm 0.04 \pm 0.11
\end{aligned} \tag{15}
$$

where the third error on $\sin 2\beta$ is due to the uncertainty in the $CP$-even content. As with the $\phi K^0$ results the central value of $\sin 2\beta$ is slightly lower than the SM value but agrees within errors. The $C$ value is again zero within errors. The time-dependent asymmetries for this mode as well as $\phi K^0_S$ and $\phi K^0_L$ are shown in fig. 6.

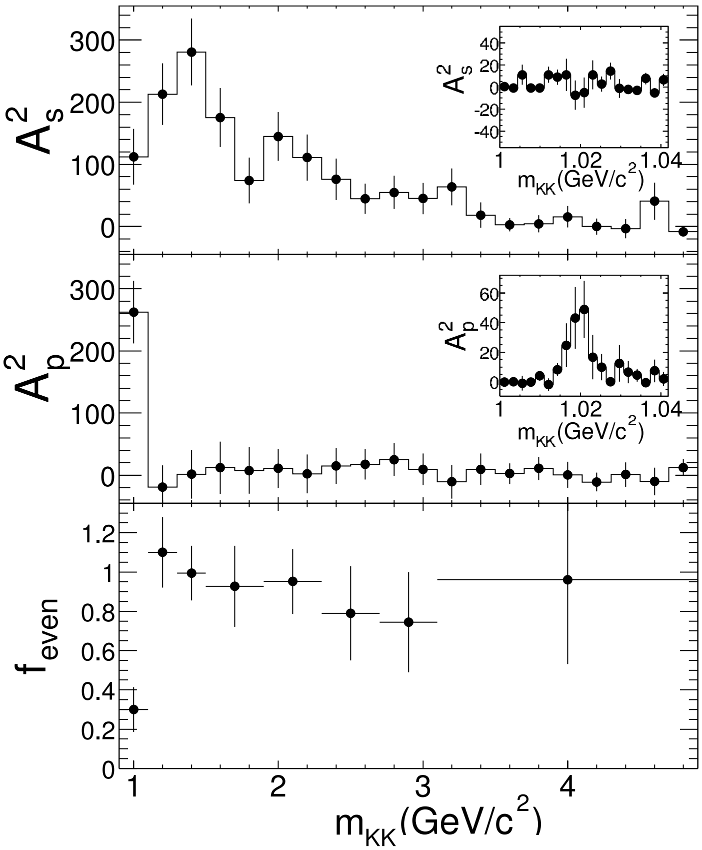


Figure 5: S- and P-wave intensities and $CP$-even fraction as a function of $K^+K^-$ mass.

#### 2.2.3 $B^0 \to K^0_S K^0_S K^0_S$

This mode, like $\phi K^0$, is very clean from a theoretical standpoint. It is also a pure $CP$-even state making the experimental determination simpler. An experimental complication is that there are no tracks originating from the primary vertex and as such the determination of the vertex separation (essential for a time-dependent analysis) was thought to be impossible. However, it was found in the *BABAR* analysis of $B^0 \to K^0_S \pi^0$ that applying a beam-spot constraint allows successful vertexing with reasonable errors[11]. Firstly a branching fraction fit is performed that only uses kinematic and event topology variables and then a time-dependent $CP$ fit is performed[12]. The branching fraction fit yields $88 \pm 10$ signal events from a data sample of 227 million $B\overline{B}$ pairs, which gives the following branching fraction: $\mathcal{B}(B^0 \to K^0_S K^0_S K^0_S) = (6.9\,^{+\,0.9}_{-\,0.8} \pm 0.6) \times 10^{-6}$ The $CP$ fit gives the following results:

$$\begin{aligned} S_{K^0_S K^0_S K^0_S} &= -0.71\,^{+\,0.38}_{-\,0.32} \pm 0.04 \\ C_{K^0_S K^0_S K^0_S} &= -0.34\,^{+\,0.28}_{-\,0.25} \pm 0.05 \\ \sin 2\beta_{\text{eff}} &= +0.79\,^{+\,0.29}_{-\,0.36} \pm 0.04 \end{aligned} \tag{16}$$

Again, these results are highly consistent with the SM value of $\sin 2\beta$. The distributions of $\Delta t$ for $B^0$ and $\overline{B}^0$ tagged events are shown in fig. 7 along with the time-dependent asymmetry.

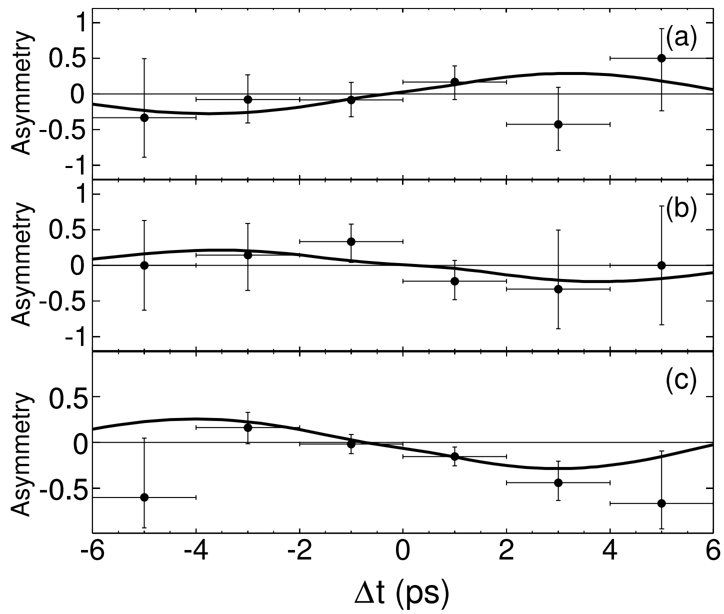


Figure 6: Time-dependent asymmetry distributions for (a) $\phi K_S^0$, (b) $\phi K_L^0$ and (c) $K^+K^-K_S^0$ excluding $\phi K_S^0$. The signal to background ratio is enhanced by a cut on the likelihood ratio.

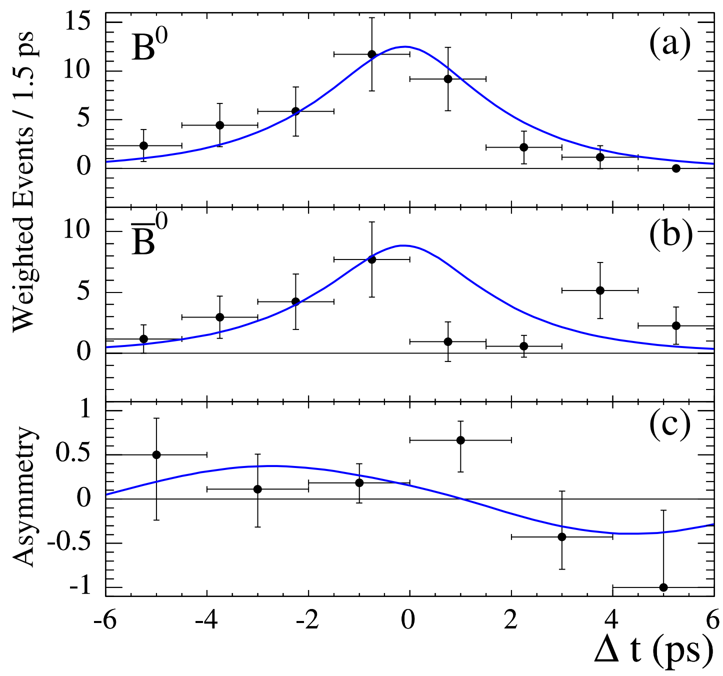


Figure 7: Time-dependent distributions for $B^0 \to K_S^0\ K_S^0\ K_S^0$.

### 2.2.4 *Summary of* sin2$\beta$ *from* $b \to s\bar{s}s$ *Penguin Modes*

The results presented above are all consistent with the value of sin2$\beta$ measured in the charmonium modes. However, there are measurements in the penguin modes that are not so consistent, shown in fig. 8, and the average of all the penguin modes differs from the average of the charmonium modes by $3.7\sigma$. It must be emphasised, however, that the theoretical uncertainty on many of the modes is high, so large deviations may be possible within the Standard Model. More precise measurements of these modes, particularly the most clean modes such as $\phi K^0$, are necessary before any conclusions can be drawn about the presence of New Physics.

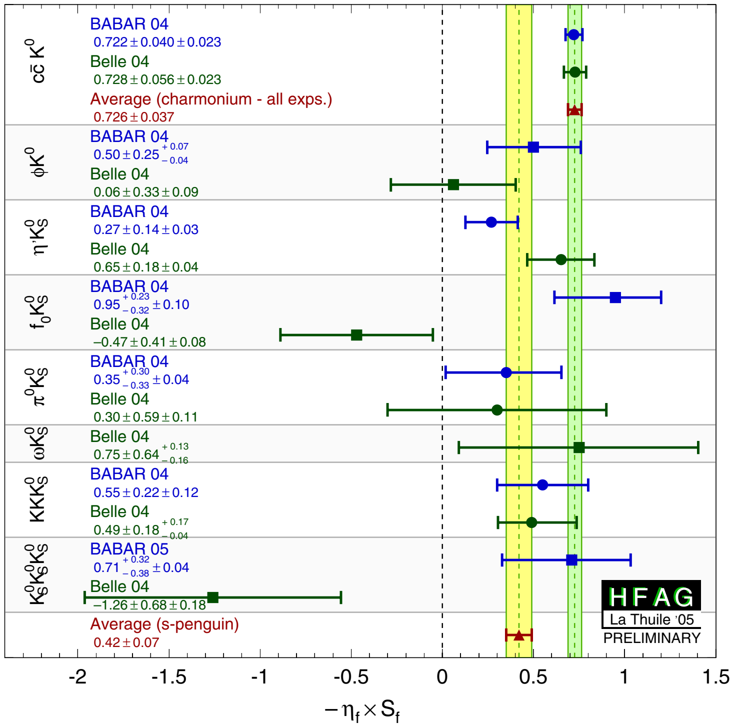


Figure 8: Comparison of sin2$\beta$ measured in charmonium and $b \to s\bar{s}s$ penguin modes

## 3 Measurements relating to $\alpha$

The decays of neutral $B$ mesons to the final states $hh$, where $h = \rho, \pi$, are sensitive to the CKM angle $\alpha$ in the interference between decay and mixing. The presence of penguin loop diagrams complicates the situation by introducing additional phases such that the measured parameter is $\alpha_{\text{eff}} = \alpha + \delta\alpha_{\text{penguin}}$. In terms of the time-dependent asymmetry defined in eq. (13) the coefficients are given by:

$$S_{hh} = \frac{2\text{Im}(\lambda_{hh})}{1 + |\lambda_{hh}|^2}, \quad C_{hh} = \frac{1 - |\lambda_{hh}|^2}{1 + |\lambda_{hh}|^2} \tag{17}$$

and $\lambda_{hh}$ is given by:

$$\lambda_{hh} = \frac{q}{p}\frac{\bar{A}}{A} = e^{2i\alpha}\frac{1 - \frac{P}{T}e^{-i\alpha}}{1 - \frac{P}{T}e^{+i\alpha}} = |\lambda|e^{2i\alpha_{\text{eff}}} \tag{18}$$

where $q$ and $p$ are the $B$ mixing coefficients and $\frac{P}{T}$ is the penguin to tree amplitude ratio, which can be different for $\pi\pi$, $\rho\pi$ and $\rho\rho$.

### 3.1 Isospin analysis in $B \to hh$

Taking the case of $B \to \pi\pi$ we can see how isospin symmetry can be employed to disentangle $\alpha$ from $\alpha_{\text{eff}}$. The following relations can be formed relating the amplitudes for the decays of $B^0$ and $\overline{B}^0$ mesons to various $\pi\pi$ final states[14]:

$$\frac{1}{\sqrt{2}}A^{+-} = A^{+0} - A^{00}, \quad \frac{1}{\sqrt{2}}\bar{A}^{+-} = \bar{A}^{+0} - \bar{A}^{00} \tag{19}$$

By also noting that

$$\left|A^{+0}\right| = \left|\bar{A}^{+0}\right| \tag{20}$$

(in the absence of electroweak penguin diagrams) it can be seen that these decay amplitudes form two triangles with a common base in the complex plane as illustrated in fig. 9.

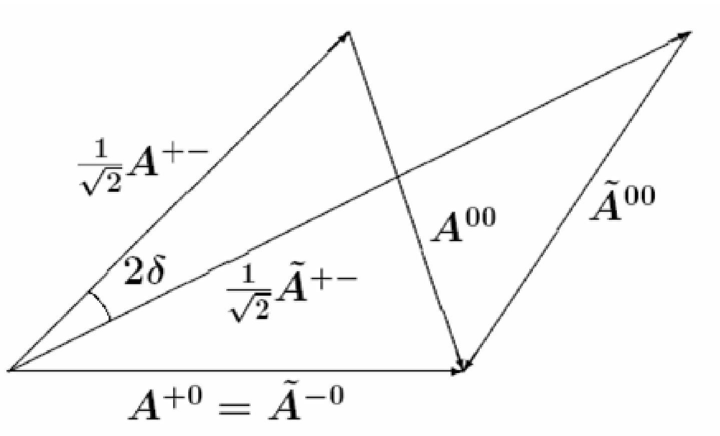


Figure 9: Illustration of the $B \to \pi\pi$ isospin triangles. $\delta = |\alpha - \alpha_{\text{eff}}|$.

For the modes $B \to \rho\rho$ there can be up to three such triangles depending on the angular structure of the decays and for $B \to \rho\pi$ a pentagon isospin analysis is required[15] or a Dalitz plot analysis[16].

### 3.2 $B \to \pi\pi$

As seen in the last section this is the simplest set of decay modes to study when attempting to measure $\alpha$. The measurements of the various branching fractions and $CP$ asymmetries are summarised in tab. 1, where $S$ and $C$ are the coefficients are defined in eq. (17) and $\mathcal{A}_{CP}$ is the charge (tag) asymmetry in the case of a charged (neutral) $B$ decay. All the measurements are sufficiently well established to perform an isospin analysis. However, the value of $\mathcal{B}(B \to \pi^0\pi^0)$ is

Table 1: *Summary of BABAR measurements of $B \to \pi\pi$ decays.*

| Mode | $\mathcal{B} \times 10^{-6}$ | $S$ | $C$ |
|---|---|---|---|
| $\pi^+\pi^-$ | $4.7 \pm 0.6 \pm 0.2$ | $-0.30 \pm 0.17 \pm 0.03$ | $-0.09 \pm 0.15 \pm 0.04$ |
| | | $\mathcal{A}_{CP}$ | |
| $\pi^\pm\pi^0$ | $5.8 \pm 0.6 \pm 0.4$ | $-0.01 \pm 0.10 \pm 0.02$ | |
| $\pi^0\pi^0$ | $1.17 \pm 0.32 \pm 0.10$ | $-0.12 \pm 0.56 \pm 0.06$ | |

Table 2: *Summary of BABAR measurements of $B \to \rho\rho$ decays.*

| Mode | $\mathcal{B} \times 10^{-6}$ | $f_L$ | $S$ | $C$ |
|---|---|---|---|---|
| $\rho^+\rho^-$ | $30 \pm 4 \pm 5$ | $0.99 \pm 0.03 \pm 0.04$ | $-0.19 \pm 0.33 \pm 0.11$ | $-0.23 \pm 0.24 \pm 0.14$ |
| | | | $\mathcal{A}_{CP}$ | |
| $\rho^\pm\rho^0$ | $22.5^{+5.7}_{-5.4} \pm 5.8$ | $0.97^{+0.03}_{-0.07} \pm 0.04$ | $-0.19 \pm 0.23 \pm 0.03$ | |
| $\rho^0\rho^0$ | $< 1.1$ 90% C.L. | — | — | |

the limiting factor in this analysis. Its value is too large to allow a tight bound to be placed on $|\alpha - \alpha_{\rm eff}|$ but it isn't sufficiently large to allow a precision measurement of this quantity with the current statistics. The limit that results from the current isospin analysis is: $|\alpha - \alpha_{\rm eff}| < 35^\circ$ at 90% confidence level[13].

### 3.3 $B \to \rho\rho$

The analysis of $B \to \rho\rho$ is potentially highly complicated due to the fact that there are three possible helicity states for the decay. The helicity zero state, which corresponds to longitudinal polarisation of the decay, is *CP*-even but the helicity $\pm 1$ states are not *CP* eigenstates. Fortunately this complication is avoided due to the experimental determination that the longitudinally polarised fraction $f_L$ is dominant[17, 18]. This and other $\rho\rho$ measurements are summarised in tab. 2[19, 20]. The measurements of the branching fractions of $B \to \rho^\pm\rho^0$ and $B \to \rho^0\rho^0$ indicate that the penguin pollution is small in these modes compared with $B \to \pi\pi$. As such it is possible to perform an isospin analysis on the longitudinal part of the decay and to place a much tighter bound on $|\alpha - \alpha_{\rm eff}|$, at the same time as using the results of the *CP* fit to constrain $\alpha$. From this analysis *BABAR* obtains the confidence level plot shown in fig. 10 and the measurement[20]:

$$\alpha = (96 \pm 10 \pm 5 \pm 11)^\circ \tag{21}$$

### 3.4 $B \to \rho\pi$

Previous measurements of this mode have been made using a "quasi-two-body" approach[21], i.e. cutting out the interference regions of the Dalitz plot (DP) and analysing the regions containing the $\rho$ resonances. This approach has the advantage that it avoids the need to understand the interference effects but by cutting out those regions of the DP statistical power is lost. Additionally, the statistics available to the $B$ factories are not sufficient to perform the pentagon isospin analysis that is necessary in these modes. The measurements reported here are the results of the first attempt by either of the $B$ factories to perform a time-dependent Dalitz plot analysis of a $B$ decay

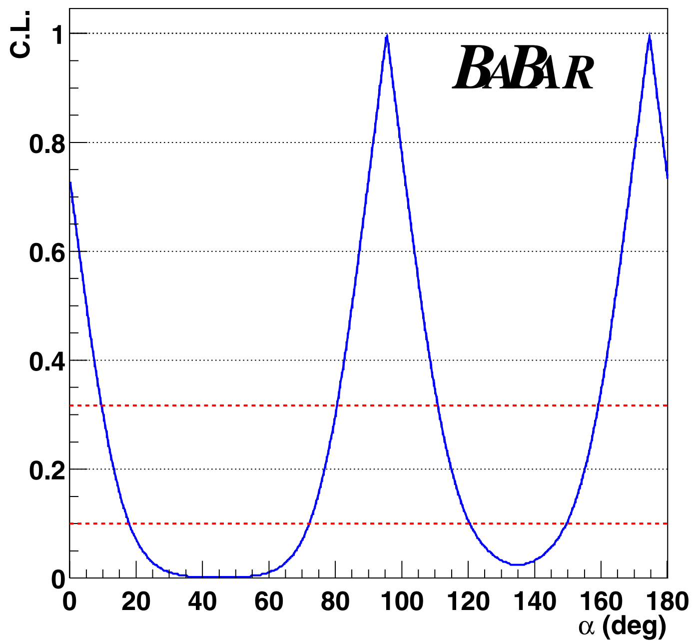


Figure 10: Plot of the confidence level of the CKM angle $\alpha$ from the *BABAR* isospin analysis of $B \to \rho\rho$.

mode[22]. This Dalitz analysis models the interference between the intersecting $\rho$ resonance bands and so determines the strong phase differences from the Dalitz plot structure. The Dalitz amplitudes and time-dependence are all contained in various complex parameters within the likelihood fit. The values obtained for these parameters are then converted back into the quasi-two-body *CP* observables, which are more intuitive in their interpretation and are defined in[21]:

$$\begin{aligned} S &= -0.10 \pm 0.14 \pm 0.04 \\ C &= 0.34 \pm 0.11 \pm 0.05 \\ \mathcal{A}_{CP} &= -0.088 \pm 0.049 \pm 0.013 \end{aligned} \tag{22}$$

Using isospin with these results the confidence level plot shown in fig. 11 is obtained and the following constraint is placed on $\alpha$:

$$\alpha = (113^{+27}_{-17} \pm 6)^{\circ}. \tag{23}$$

This result is of particular value because there is a unique solution between 0 and 180°, which helps to break the ambiguity on the $\rho\rho$ result, which is in itself more precise. The direct *CP* violation parameters $C$ and $\mathcal{A}_{CP}$ can be combined into more intuitive variables $A^{+-}_{\rho\pi}$ and $A^{-+}_{\rho\pi}$, which give the charge asymmetry in the modes where the $\rho$ and the $\pi$ respectively is emitted by the $W$ boson. The contour plot for these observables can be found in fig. 12, which shows that there is a hint of direct *CP* violation at the $2.9\sigma$ level.

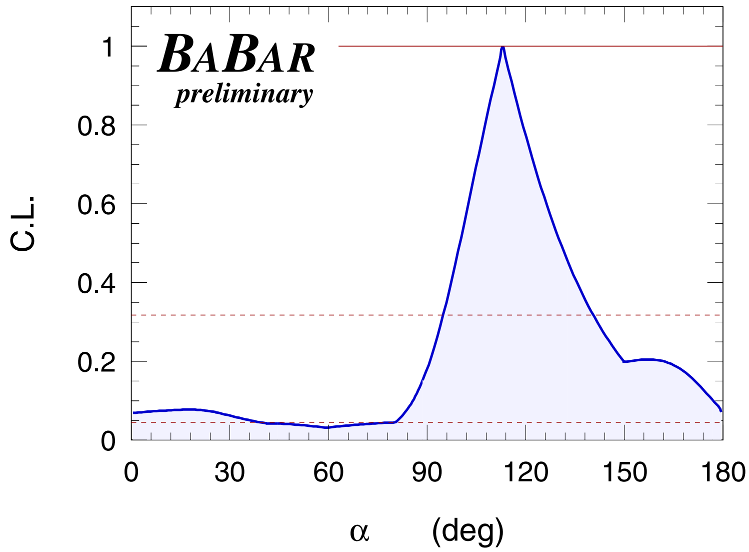


Figure 11: Plot of the confidence level of the CKM angle $\alpha$ from the *BABAR* isospin analysis of $B \to \rho\pi$.

### 3.5 Combined results for $\alpha$

Combining all the *BABAR* results on $\alpha$ presented above gives the measurement:

$$\alpha = (103^{+11}_{-10})^{\circ}. \tag{24}$$

The confidence level plot of each individual measurement and the combined result is shown in fig. 13. Also included in the plot is the result for $\alpha$ from the global CKM fit not including the direct constraints from these results. The agreement is excellent.

## 4 Measurements relating to $\gamma$

Sensitivity to the CKM angle $\gamma$ occurs in decay modes that have contributions from diagrams containing $b \to c$ and $b \to u$ transitions that interfere with one another. The size of the interference, and hence the sensitivity to $\gamma$, is determined by the relative magnitudes of the two processes. The two diagrams being considered here are those of $B^+ \to \overline{D}^0 K^+$ and $B^+ \to D^0 K^+$, which are illustrated in fig. 14. In order for these two processes to interfere it is required that the final state be the same. Here we examine the decay of the $D^0$ and $\overline{D}^0$ to $K^0_S \pi^+ \pi^-$.

In this decay mode, there are four unknowns

- $\gamma$,
- $r_B = \frac{|A(B^+ \to D^0 K^+)|}{|A(B^+ \to \overline{D}^0 K^+)|}$
- $\delta_B$ - the strong phase of the $B$ decay and

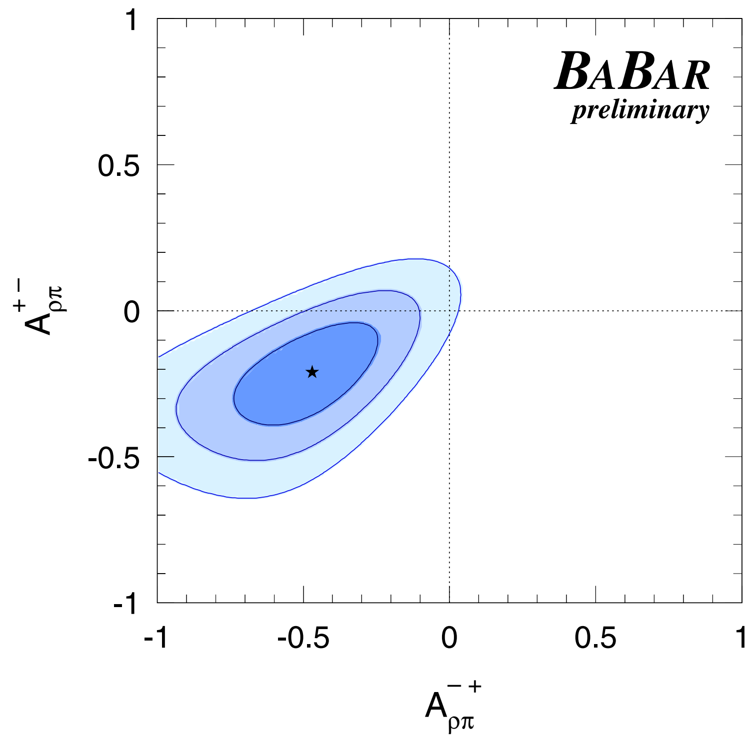


Figure 12: Plot of the confidence level contours for the direct *CP* violation observables $A_{\rho\pi}^{+-}$ and $A_{\rho\pi}^{-+}$.

- $\delta_D$ - the strong phase of the $D$ decay.

This last parameter is eliminated by using the Dalitz plot structure of the $D^0 \to K_S^0\pi^+\pi^-$ decay in the likelihood fit. This is determined by performing a full Dalitz plot analysis of this $D$ decay mode using a very high statistics sample of $D^{*+}$ decays. The resulting amplitude model is then fixed and used as the $f$ terms in the following expressions:

$$\begin{aligned} M_+(m_-^2, m_+^2) &= \left|A(B^+ \to \overline{D}^0 K^+)\right| \left[f(m_+^2, m_-^2) + r_B e^{i\delta_B} e^{i\gamma} f(m_-^2, m_+^2)\right] \\ M_-(m_-^2, m_+^2) &= \left|A(B^- \to D^0 K^-)\right| \left[f(m_-^2, m_+^2) + r_B e^{i\delta_B} e^{i\gamma} f(m_+^2, m_-^2)\right] \end{aligned} \tag{25}$$

The fit to the $D^*$ sample can be seen in fig. 15.

A simultaneous fit is then performed to both the $B^+$ and $B^-$ data samples in order to determine $\gamma$, $\delta_B$ and $r_B$. In addition to the Dalitz plot information, kinematic and event topology information is used to separate the signal and background events. The number of signal events was found to be $261 \pm 19$ for the $D^0K^+$ mode, $83 \pm 11$ for the $D^{*0}(D^0\pi^0)K^+$ mode and $40 \pm 8$ for $D^{*0}(D^0\gamma)K^+$. The results determined are[23]:

$$\begin{aligned} r_B < 0.19\,(90\%\text{CL}), \quad \mathrm{r_B^*} &= 0.155\,^{+0.070}_{-0.077} \pm 0.040 \pm 0.020 \\ \delta_B = (114 \pm 41 \pm 8 \pm 10)^\circ, \quad \delta_B^* &= (303 \pm 34 \pm 14 \pm 10)^\circ \\ \gamma &= (70 \pm 26 \pm 10 \pm 10)^\circ. \end{aligned} \tag{26}$$

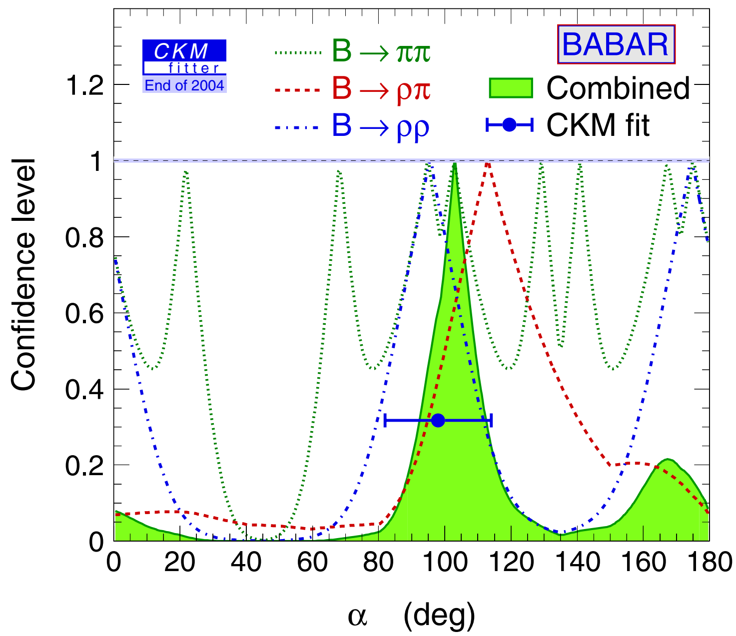


Figure 13: Plot of the confidence level contours for the CKM angle $\alpha$ using all *BABAR* measurements as an input. The blue point with error bar is the result of the full CKM fit without the direct constraints on $\alpha$.

## 5 Summary

In the last few years the measurements of the angles of the CKM Unitarity Triangle from the *BABAR* experiment have become increasingly sophisticated and precise. New techniques are allowing ambiguities to be resolved and measurements to be performed in modes that were not thought possible when the $B$ factories were first conceived. The measurements are mostly in excellent agreement with the Standard Model predictions but there are possible hints of New Physics in the measurements of sin2$\beta$ in $b \to s$ penguin modes. *BABAR* intends to double its dataset by Summer 2006 and again by 2008 so we can look forward to further improvement in the measurements of these parameters.

## 6 Acknowledgements

Many thanks to Adrian Bevan, Paul Harrison and Andreas Hoecker for their advice and assistance in the preparation of this presentation and manuscript. This work is funded in part by the Particle Physics and Astronomy Research Council, United Kingdom.

## References

[1] M. Kobayashi and T. Maskawa, Prog. Theor. Phys. **49**, 652 (1973).

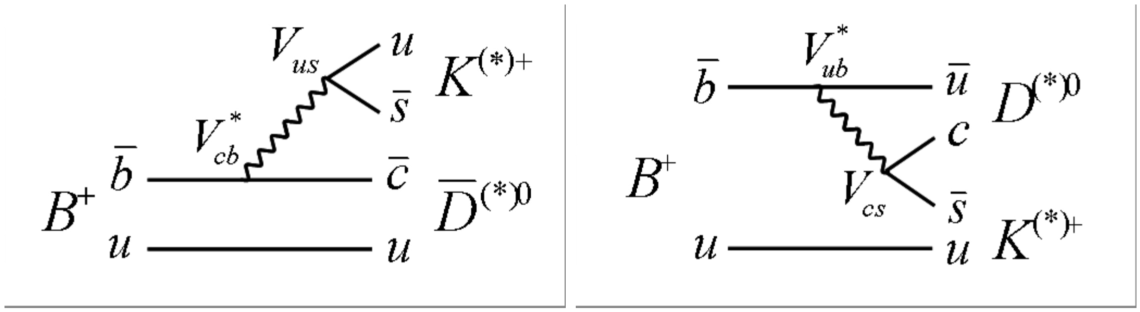


Figure 14: Diagrams for the decays $B^+ \to \overline{D}^0 K^+$ and $B^+ \to D^0 K^+$, which are sensitive to the angle $\gamma$ in their interference if the $D^0$ and $\overline{D}^0$ decay to the same final state.

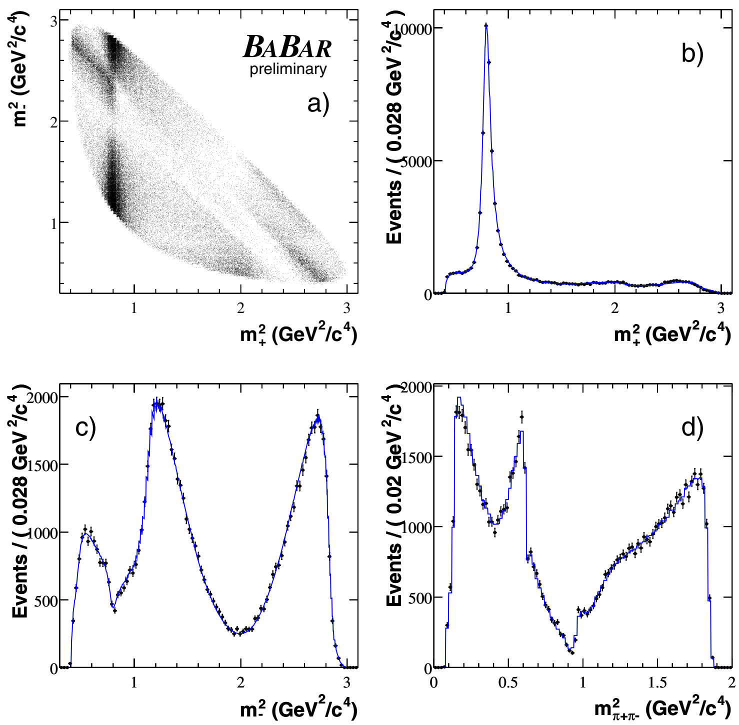


Figure 15: (a) The $D^0 \to K^0_S\pi^+\pi^-$ Dalitz distribution from $D^*$ decays. Also shown are the projections onto the Dalitz variables (b) $m^2_+ = m^2_{K^0_S\pi^+}$, (c) $m^2_- = m^2_{K^0_S\pi^-}$ and (d) $m^2_{\pi^+\pi^-}$. The fit result is overlaid on the projections as a solid line.


[2] L. Wolfenstein, Phys. Rev. Lett. **51**, 1945 (1983).

[3] B. Aubert *et al.* [*BABAR* Collaboration], Nucl. Instrum. Meth. A **479**, 1 (2002).

[4] W. Kozanecki, Nucl. Instrum. Meth. A **446**, 59 (2000).

[5] B. Aubert *et al.* [*BABAR* Collaboration], Phys. Rev. Lett. **94**, 161803 (2005).

[6] B. Aubert *et al.* [*BABAR* Collaboration], Phys. Rev. D **71**, 032005 (2005).

[7] D. Aston *et al.*, Nucl. Phys. B **296**, 493 (1988).

[8] E. P. Wigner, Phys. Rev. **98**, 145-147 (1955).

[9] B. Aubert *et al.* [*BABAR* Collaboration], arXiv:hep-ex/0502019.

[10] M. Pivk and F. R. Le Diberder, arXiv:physics/0402083.

[11] B. Aubert *et al.* [*BABAR* Collaboration], Phys. Rev. Lett. **93**, 131805 (2004).

[12] B. Aubert *et al.* [*BABAR* Collaboration], arXiv:hep-ex/0502013.

[13] B. Aubert *et al.* [*BABAR* Collaboration], arXiv:hep-ex/0412037.

[14] M. Gronau and D. London, Phys. Rev. Lett. **65**, 3381 (1990).

[15] H. J. Lipkin, Y. Nir, H. R. Quinn and A. Snyder, Phys. Rev. D **44**, 1454 (1991).

[16] A. E. Snyder and H. R. Quinn, Phys. Rev. D **48**, 2139 (1993).

[17] B. Aubert *et al.* [*BABAR* Collaboration], Phys. Rev. Lett. **93**, 231801 (2004).

[18] B. Aubert *et al.* [*BABAR* Collaboration], Phys. Rev. Lett. **91**, 171802 (2003).

[19] L. Roos [*BABAR* Collaboration], arXiv:hep-ex/0407051.

[20] B. Aubert *et al.* [*BABAR* Collaboration], arXiv:hep-ex/0408061.

[21] B. Aubert *et al.* [*BABAR* Collaboration], Phys. Rev. Lett. **91**, 201802 (2003).

[22] B. Aubert *et al.* [*BABAR* Collaboration], arXiv:hep-ex/0408099.

[23] B. Aubert *et al.* [*BABAR* Collaboration], arXiv:hep-ex/0408088.